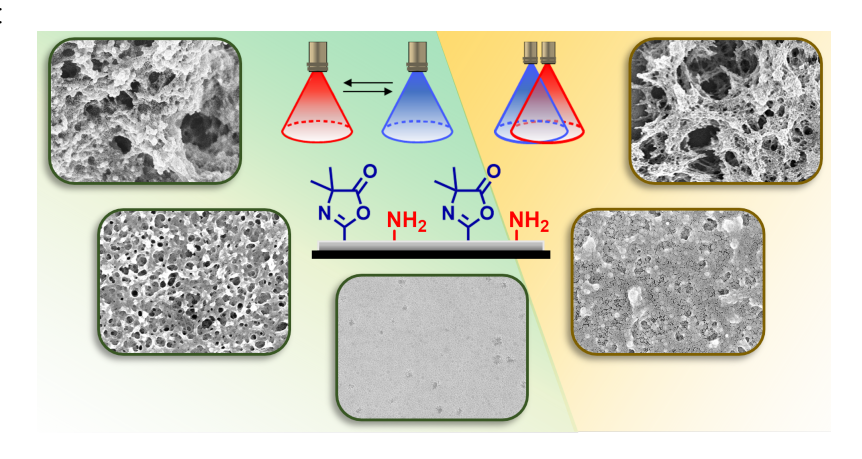
# Reactive Multilayers and Coatings Fabricated by Spray Assembly: Influence of Polymer Structure and Process Parameters on Multi-Scale Structure and Interfacial Properties

Harshit Agarwal, William M. Breining, Gabriel Sánchez-Velázquez, and David M. Lynn<sup>1,2,\*</sup>

ABSTRACT: We report new alternating and simultaneous spray-based approaches to the assembly of thin films and chemically reactive polymer coatings using azlactone- and aminecontaining building blocks. Our results reveal the impacts of both polymer structure (e.g., the presence or absence of hydrolyzed azlactone groups) and other spray-process parameters (e.g., number of cycles, elimination of rinses, and changes in spray rate) on key aspects of film growth and morphology that are relevant to potential applications of these reactive materials. Manipulation of these parameters permits rapid and automated fabrication of uniform and continuous coatings that are either (i) thin and optically transparent or (ii) thicker and optically opaque, with varying and useful levels of nano- and microscale roughness and porosity. These coatings also present both unreacted azlactone and amine functionality, allowing facile postfabrication functionalization using amine-based nucleophiles and/or electrophilic amine-reactive species. These combinations of control over physical and chemical features permit facile tuning of interfacial properties and chemical patterning to design soft material coatings with useful properties, including extreme wetting and slippery anti-fouling behaviors. These spray-based methods are fast, efficient, and amenable to coating substrates of arbitrary shape and size. The approaches reported here should thus help guide the development of new processes for the fabrication of these reactive materials that can be implemented at-scale or as elements of commercial or industrial processes.

For Table of Contents Use Only:



<sup>&</sup>lt;sup>1</sup>Department of Chemical & Biological Engineering, University of Wisconsin-Madison, 1415 Engineering Dr., Madison, WI 53706, USA; <sup>2</sup>Department of Chemistry, University of Wisconsin-Madison, 1101 University Ave., Madison, WI 53706, USA. E-Mail: (D.M.L) dlynn@engr.wisc.edu

## Introduction

Coatings that impart new properties or behaviors to surfaces, such as resistance to fouling, changes in wetting behavior, or responsiveness to stimuli, are useful in a broad range of applied contexts. Chemically reactive coatings and reactive coating processes are particularly versatile in this regard because they (i) permit chemical functionalization or patterning of surface features and, thus, tailoring of interfacial properties after fabrication, and (ii) can provide routes to crosslinking and promote aspects of structure formation in ways that can lead to desirable physical properties and enhance stability in harsh environments. Many methods have been developed for this purpose, including both gas-phase (e.g., chemical vapor deposition; CVD) and solution-phase approaches (e.g., dip-coating, spin-coating, and spray-coating) that can be readily integrated into commercial and industrial processes.

The work reported here was motivated broadly by methods for the layer-by-layer (LbL) assembly of polymer multilayers. <sup>1,2</sup> These approaches are extraordinarily versatile and can be used to fabricate composite or multicomponent coatings using a broad range of polymer-based building blocks and either non-covalent interactions <sup>3-6</sup> or covalent bond-forming reactions <sup>4,7-11</sup> that occur between them. LbL processes also allow structural features (e.g., film thickness and porosity) and compositional complexity to be varied by manipulation of many different process parameters, including the structure and properties of the constituent polymers and the number of assembly cycles. <sup>1,2,12</sup> As one example of relevance to this study, we reported previously that interfacial reactions between the amine-reactive polymer poly(2-vinyl-4,4-dimethylazlactone) (PVDMA; Figure 1) and the amine-containing polymer poly(ethyleneimine) (PEI; Figure 1) can drive LbL assembly into films that are either (i) thin, smooth, and relatively featureless at the nanometer scale, <sup>13-15</sup> or (ii) thicker and possessing salient nano- and microscale surface features

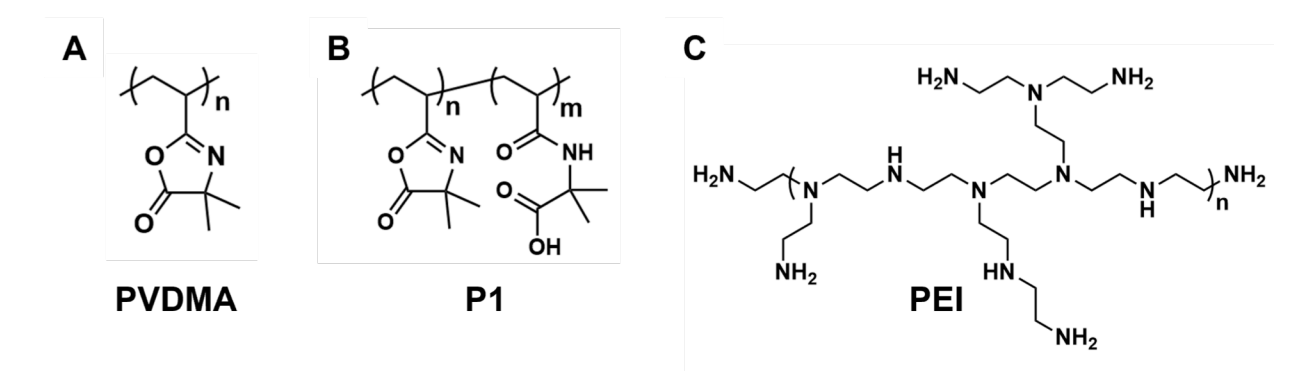


**Figure 1.** Structures of (A) poly(2-vinyl-4,4-dimethylazlactone) (PVDMA), (B) a copolymer derivative of PVDMA containing carboxylic acid-functionalized side chains, obtained by partial side-chain azlactone hydrolysis of PVDMA (**P1**; m=0.22), and (C) branched poly(ethyleneimine) (PEI), the polymer used as an amine-containing building block in this study.

that lead to coatings with surface or bulk properties (e.g., anti-fouling or anti-wetting behaviors and stability in complex media)<sup>16-18</sup> of potential utility in many different applications. We note, however, that this past work and many other conventional LbL processes involve the repetitive immersion of substrates into solutions of polymer building blocks—a process that is time-consuming, cumbersome, and, in general, challenging to implement on a commercial scale or for the coating of larger objects. <sup>19-21</sup>

The introduction of spray-assisted methods for LbL assembly has resulted in significant practical advances, enabling the deposition and patterning of thin films and coatings over large areas, on substrates of arbitrary size and shape, and in industrial and commercial contexts. <sup>19-24</sup> In addition to practical gains related to efficiency and scale, these spray-based methods also introduce many new process parameters (e.g., spray velocity and angle, droplet size, etc.) <sup>25-29</sup> and enable fundamentally new approaches, including those involving simultaneous spraying, <sup>30-32</sup> that can be used to tune film morphologies and resulting functional behaviors. <sup>19-21,33,34</sup> The work reported here was motivated by the broad goal of understanding relationships between spray process parameters and elements of polymer structure and chemical reactivity that influence

assembly and govern structure formation in coatings comprised of azlactone-containing polymers.

Here, we report new approaches to the spray-based assembly of chemically reactive coatings fabricated using PVDMA and copolymers of PVDMA. These spray-based methods enable (i) traditional LbL (i.e., alternate spraying) approaches to reactive assembly that are conceptually similar to conventional sequential-immersion processes, as well as (ii) the introduction of new processes that permit simultaneous spraying of reactive building blocks to construct multicomponent reactive films. We also characterized the influence of structural features and process parameters that impact film growth and structure formation in these sprayassembled films in ways that are important in potential practical applications of these materials. We demonstrate that judicious manipulation of these parameters enables the assembly of uniform coatings with a wide variety of morphologies and surface features (e.g., ranging from thin, smooth, and optically transparent to thick, rough, and nanoporous) using automated processes that are faster, more reproducible, and more amenable to scale-up and adoption in processes for continuous manufacturing than immersion-based methods. Finally, we demonstrate that these spray-assisted methods lead to the retention of both reactive azlactone and reactive amine functionality, thereby permitting the rapid and continuous coating of objects that can be chemically functionalized, post-fabrication, using a wide range of nucleophilic and electrophilic functional groups to impart useful (e.g., anti-fouling, non-wetting, or chemically patterned) interfacial properties. The results of these experiments provide insights, guiding principles, and new experimental methods that are useful for tuning and tailoring the properties and behaviors of azlactone-based coatings, and advance toward an important long-term goal of developing processes for the fabrication of these materials that can be adopted and implemented at-scale in commercial and industrial processes.

## **Materials and Methods**

Materials. Branched poly(ethyleneimine) (PEI, MW ~25 000), acetone (ACS reagent grade), dimethyl sulfoxide (DMSO, ACS reagent grade), N,N-dimethylformamide (DMF, ACS reagent grade), dimethylaminopropylamine (DMAPA), 1-aminodecane (*n*-decylamine), hexamethylenediamine, (3-aminopropyl)triethoxysilane (APTES, 99%), silicone oil (for oil baths), propylamine (98%), propionyl chloride (98%), decanoyl chloride (98%), N,Ndiisopropylethylamine (Hünig's base, ≥ 99 %), silica nanoparticle dispersions in water (<50 nm, triethoxylpropylaminosilane-functionalized), and toluene (ACS reagent grade) were purchased from Sigma Aldrich (Milwaukee, WI). Eutrophic lake water was locally sourced from Lake Mendota, Madison, WI. Nature's Touch skim milk was purchased from Kwik Trip (Madison, WI). Pooled human urine was purchased from Innovative Research Inc. (Novi, MI). Ethanol (EtOH, 200 proof) was obtained from Decon Laboratories (King of Prussia, PA). Double IPA beer (Double Dog; Flying Dog Brewery) was purchased from a local liquor store (Madison, WI). Yogurt drink (Chobani mixed berry Greek yogurt drink) and Soy Sauce (Kroger) were purchased from Pick' n Save (Madison, WI). Fresh porcine blood was collected in a 50 mL conical centrifuge tube containing 3.4% sodium citrate in PBS at a ratio of 9:1 (blood:citrate) and stored in a refrigerator until use. Wire mesh was purchased from Gerard Daniel Worldwide, Inc. (Hanover, PA). Silicon wafers (4 in) were purchased from Silicon Inc. (Boise, ID). Silicon substrates used for reflective infrared spectroscopy experiments were prepared by depositing thin layers of titanium (10 nm) and gold (200 nm) sequentially onto clean silicon wafers using an

electron-beam evaporator. PDMS (SYLGARD™ 184) was purchased from Dow, Inc. (Midland, MI). Flexible polyester films (Grafix Dura-Lar; 0.005 in) were obtained from Amazon.com, Inc. (Seattle, WA). Tetrahydrofuran (THF, ACS reagent grade), wide-mouthed glass containers (30 mL), polyethylene tubing (1/8″ ID × 1/4″ OD × .062″), Cytiva Whatman™ filter paper (grade 2), and glass microscope slides (Corning) were purchased from Fisher Scientific (Pittsburgh, PA). 2-Vinyl-4,4-dimethyl azlactone (VDMA) was a kind gift from Dr. Steven M. Heilmann (3M Corporation, Minneapolis, MN). Poly(2-vinyl-4,4-dimethyl azlactone) (MW ~53, 000; PDI = 4.1) and P1 (MW ~70,100; PDI = 3.8; 22% hydrolyzed) were synthesized by the free-radical polymerization of freshly distilled and undistilled VDMA, respectively, using procedures described previously. <sup>35,36</sup> Tetramethylrhodamine cadaverine (TMR-cadaverine) was purchased from Invitrogen (Carlsbad, CA). 7-Hydroxycoumarin-3-carboxylic acid N-succinimidyl ester was purchased from ThermoFisher Scientific (Waltham, MA). Jeffamine® T-403 was a gift sample from the Huntsman Corporation (The Woodlands, TX). All materials were used as received without further purification unless noted otherwise.

General Considerations. Compressed air used to dry samples was filtered through a  $0.2~\mu m$  membrane syringe filter. Scanning electron micrographs were acquired using a LEO 1550 SEM at an accelerating voltage of 3 kV using an in-lens SEM detector. Coated planar surfaces were cut into  $0.5 \times 0.5$  cm sections for top-down SEM imaging. For cross-sectional SEM images, the substrates were scored on the back and then manually broken to expose the cross-section of the films. In some cases, a razor blade was used prior to imaging to scratch a pair of perpendicular lines in the films in an arbitrarily chosen location to facilitate imaging of cross-sections of the films. The samples were then mounted on a SEM stub by conductive carbon tape. Samples were

coated with a thin layer of gold using a gold sputterer operating at 10 mA under a vacuum pressure of 50 mTorr for 2 min before imaging. Digital photographs and videos were acquired using a Samsung Galaxy S8+ smartphone. For contact angle measurements, coated substrates were cut into 1×1 cm square sections. Contact angle measurements were made using a Dataphysics OCA 15 Plus contact angle goniometer at ambient temperature with 5 µL Milli-Q water droplets. The advancing and receding contact angles were measured by the droplet volume change method. Optical thicknesses of films fabricated on silicon substrates were acquired using a Gaertner LSE ellipsometer (632.8 nm, incident angle = 70°), and data points were processed using the Gaertner ellipsometer measurement software. Relative thicknesses were calculated assuming an average index of refraction of 1.4 for the multilayered films. Thicknesses were determined for at least three substrates in at least three different locations on each substrate and are presented as averages with standard deviations. Polarization modulation infrared reflectanceabsorbance spectroscopy (PM-IRRAS) was conducted in analogy to previously reported methods. 37,38 Silicon substrates used for reflective infrared (IR) spectroscopy experiments were prepared by depositing thin layers of titanium (10 nm) and gold (200 nm) sequentially on clean silicon wafers using an electron-beam evaporator (Tek-Vac Industries, Brentwood, NY). Coated silicon substrates were placed at an incident angle of 83° in a Nicolet Magna-IR 860 Fourier transform infrared spectrophotometer equipped with a photoelastic modulator (PEM-90, Hinds Instruments, Hillsboro, OR), a synchronous sampling demodulator (SSD-100, GWC Technologies, Madison, WI), and a liquid-nitrogen-cooled mercury cadmium telluride detector. For each sample, 500 scans were acquired at a resolution of 4 cm<sup>-1</sup>, and data was collected as differential reflectance vs. wavenumber. Fluorescence microscopy images were acquired using an Olympus IX70 microscope and were analyzed using the Metavue version 4.6 software

package (Universal Imaging Corporation). All data were analyzed using Microsoft Excel for Office 360 and plotted using GraphPad Prism 7 (version 7.0h).

Fabrication of Spray-Based Coatings. Glass, silicon, and gold-coated silicon slides were cut into 2×2 cm squares. All substrates were cleaned with water, ethanol, and acetone, dried under a stream of filtered and compressed air, and oxygen plasma-treated for 600s (Plasma Etch, Carson City, NV). For films fabricated using P1 and non-polymeric linkers, the silicon substrates were cleaned in the above manner and then coated with APTES to help promote adherence of the coatings to the substrates. Briefly, the cleaned slides were incubated in a 1% APTES (in toluene) solution for one hour at 70 °C. The slides were then removed and baked in an oven set at 110 °C for 15 minutes. These APTES-treated slides were then used directly or stored in a vacuum desiccator prior to use. Coatings were fabricated using an automated SPALAS<sup>TM</sup> coatings system (AGILTRON®, Woburn, MA) with different nozzles for spraying PEI, PVDMA or P1, and rinse solutions. In-house compressed air lines supplied pressurized gas with an overpressure fixed at 20 psi, and all nozzles were calibrated to flow rates of 3 ml/min  $\pm$  0.5 ml/min. The substrates were placed horizontally (8 cm from the nozzle), and solutions were sprayed perpendicularly to the substrates with horizontal movement (at a rate of 1.5 cm/s) to improve homogeneity (coating a total surface area of ~2 cm<sup>2</sup>). The tracking of the spray nozzles used during coating procedures varied according to the size and nature of the substrates being coated, but for planar substrates generally consisted of a pattern of repeating squares (see relevant figures in the main text). For coating the outside surfaces of polyethylene tubing segments, a longitudinal rod was inserted through the ends of the tubing segment to create a rotation axis perpendicular to the spray nozzles. The tubing segments were rotated at 400 rpm while the spray nozzle sprayed solutions

along the length of the tubing segments, resulting in homogenous coatings along the outside surface of the tubing segments. For coating the inside surfaces of glass containers, the container was placed horizontally on a rotating platform with a rotational axis of 45° relative to the spray nozzles. The container was rotated at 200 rpm while the spray nozzle sprayed the solutions, resulting in homogenous coatings on the inside surfaces of the containers.

The coatings were fabricated either by sequential or simultaneous spraying of dilute organic solutions of PEI and P1 or PVDMA. All polymer solutions were prepared with respect to the molecular repeat units. Sequential spraying was performed in the following general manner: (i) substrates were sprayed with a PEI solution (10 mM in DMF with respect to the molecular repeat unit) for approximately 6 s; (ii) substrates were washed by spraying with DMF for approximately 12 s; (iii) substrates were sprayed again with P1 or PVDMA solution (10 mM in DMF with respect to the molecular repeat unit) for approximately 6 s and (iv) finally, substrates were washed again with the procedure outlined in step (ii). This cycle was repeated multiple times (see main text) to fabricate multilayers consisting of P1/PEI or PVDMA/PEI layer pairs (or 'bilayers'). In one modification to the general protocol described above, the DMF rinse steps applied between spraying polymer solutions (PEI and P1 or PEI and PVDMA) were eliminated. The fabrication of multilayers using P1 and non-polymeric linkers followed the same general procedure described above, with the exception that DMSO was used as a solvent instead of DMF. Simultaneous spraying was performed by spraying both PEI and P1 solutions at different concentrations in DMF (keeping the total polymer spray rate constant at  $7.2 \pm 1.2$  mmol.s<sup>-1</sup>) through two different nozzles at the same time for different cumulative spraying times (see main text). All other substrates used in this study (polyester film, wire mesh, and filter paper) were also coated using this protocol. After fabrication, multilayers were cleaned with DMF, dried

under a stream of filtered, compressed air, and used in subsequent experiments immediately or stored in a vacuum desiccator until use. All coatings were fabricated at room temperature.

Post-Fabrication Functionalization and Chemical Patterning of Reactive Thin Films. Films containing unreacted azlactone groups, prepared as described above, were functionalized using the following general procedure. In experiments for which larger-area functionalization of the entire surface of film-coated substrates was desired, substrates coated with azlactone-containing films were immersed in solutions containing primary amine-functionalized molecules. For example, film-coated substrates were immersed in solutions of *n*-decylamine (10 mM in THF), propylamine (10 mM in THF), or DMAPA (10 mM in THF) overnight at room temperature. Functionalized films were then rinsed with THF and acetone and dried with filtered air. For experiments in which microcontact printing was used to chemically pattern micrometer-scale features, polydimethylsiloxane (PDMS) stamps consisting of an array of pillars (100 µm square) were used. Inking of the stamps was achieved by first spreading a 3 μL droplet of TMR cadaverine in DMSO (1 mg/mL) on a clean glass substrate using another glass plate to produce a thin layer. The stamp was gently placed onto the wet surface and then quickly transferred and placed gently on the surfaces of azlactone-containing films. Stamps were left in contact with the films for 30 seconds and then removed. The patterned films were then rinsed with copious amounts of DMSO and acetone and dried under a filtered air stream. Post-fabrication functionalization by chemical modification of residual amine groups was performed using the following general procedure. For functionalization using acid chlorides, coated substrates were immersed in solutions containing propionyl chloride or decanoyl chloride (20 µM in THF) and Hünig's base (30  $\mu$ M in THF) for ~ 3 hours at room temperature. The reaction of film-coated

substrates (before or after treatment with acid chloride) with amine-reactive fluorophore was performed by placing a droplet of 7-(diethylamino)coumarin-3-carboxylic acid *N*-succinimidyl ester in DMSO (2 mg/mL) on the film-coated substrate surface for 30 min at room temperature. After functionalization, the substrates were rinsed with copious amounts of DMSO, acetone, and ethanol and dried under a filtered air stream.

Preparation and Characterization of Slippery Surfaces. Porous polymer films fabricated by sequential or simultaneous spraying of P1 and PEI were treated with decylamine and decanoyl chloride, as described above, and then infused with lubricating liquids (oils) using the following general protocol. The required number of droplets of silicone oil (5  $\mu$ L) were placed onto film-coated surfaces and physically spread over the surface using weighing paper. The excess silicone oil was wiped-off by the weighing paper. For sliding time measurements, a 20  $\mu$ L water droplet was placed onto the oil-infused surface inclined at an angle of 20 degrees. The time required for the droplet to slide a distance of 2 cm was measured using a digital timer.

## **Results and Discussion**

Spray-Based LbL Assembly of Reactive Coatings Using an Azlactone-Containing Copolymer

We began our studies by investigating the spray-assisted LbL assembly of thin films using polyethyleneimine (PEI; an amine-containing polymer) and **P1**, an azlactone-functionalized copolymer synthesized by the partial hydrolysis of poly(2-vinyl-4,4-dimethyl azlactone) (PVDMA).<sup>36</sup> We previously reported that partial hydrolysis of the azlactone groups of PVDMA can contribute to structure formation and porosity on the nano- and microscale during immersion-based LbL assembly in ways that impart useful functional properties (e.g., coatings

that exhibit superhydrophobicity<sup>36</sup> or recapitulate features of other PVDMA/PEI coatings fabricated in past studies using immersion coating<sup>17,18,36</sup> that exhibit extreme wetting or antifouling properties). It was not clear at the outset of these studies whether reactive multilayer assembly (in general) or these useful levels of nanoscale structure (in particular) could also be achieved by the iterative and alternating spraying of these reactive components directly onto surfaces. We began our studies using samples of **P1** containing ~22% ring-opened, carboxylate-functionalized side chains, which is a level of hydrolysis observed to lead to nanoporosity and retention of amine reactivity when co-assembled with PEI using immersion in bulk polymer solutions.<sup>36</sup> This **P1**/PEI system provided a useful and practical model for these initial studies; additional characterization of spray-based methods using PEI and unhydrolyzed PVDMA is described in other sections below.

We fabricated P1/PEI films on the surfaces of planar substrates using an automated spray coating system with separate spray nozzles for spraying solutions of P1, PEI, and intermittent solvent rinse/wash steps. In these initial experiments, substrates were fixed horizontally, and polymer solutions were sprayed from an angle of 90° relative to the surface in a constant horizontal motion (covering a total surface area of ~ 2 cm²). A typical spray-based LbL cycle consisted of alternate and repetitive spraying of dilute organic solutions of P1 or PEI in DMF (used here as a model, non-volatile organic solvent capable of dissolving both polymers and other materials described below) for ~6 s, with intermittent solvent-only spray steps for ~12 s (Figure 2A; see Materials and Methods for additional details). Figure 2B (solid circles) shows a plot of optical thickness, as characterized by ellipsometry, versus the number of P1/PEI layers, hereafter referred to as 'bilayers,' deposited on reflective silicon substrates. The dotted line represents a linear fit to these data and reveals film thickness to increase as a linear function of

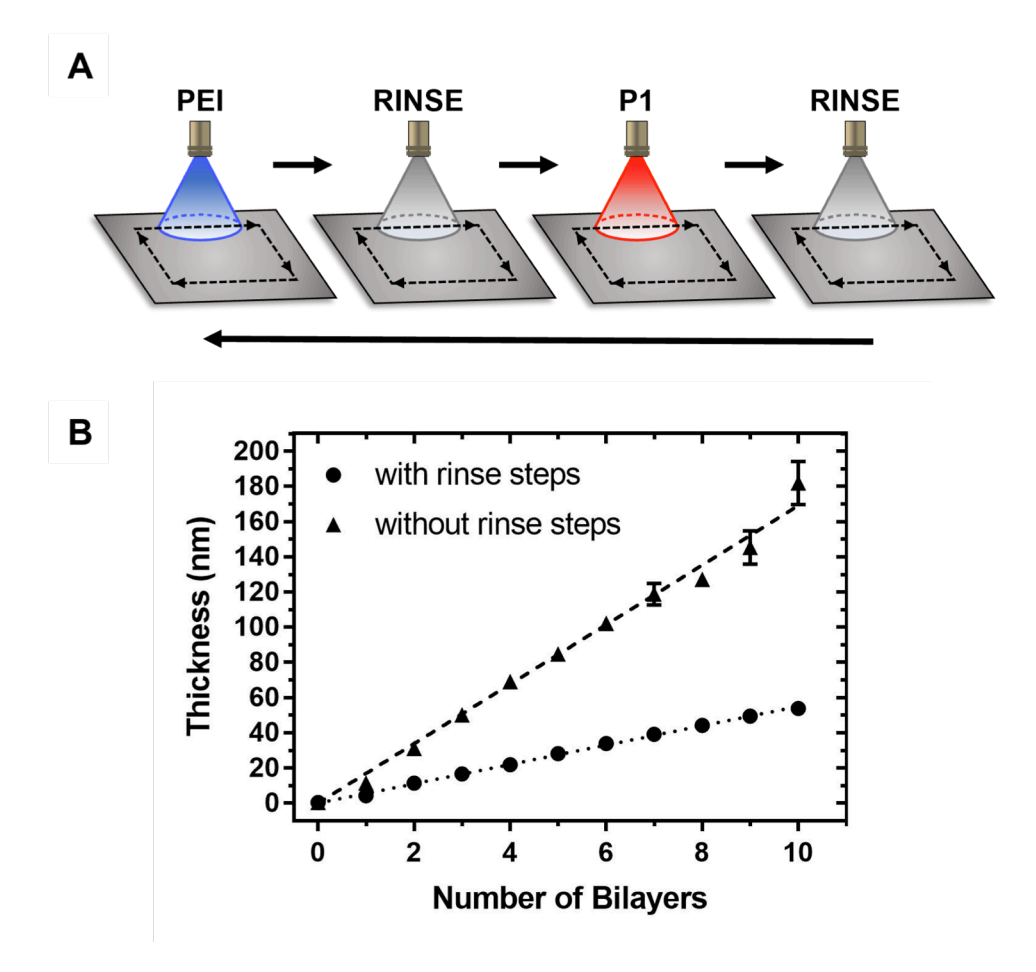


**Figure 2.** A) Schematic showing spray-coating workflow for the LbL fabrication of **P1**/PEI coatings. The dotted lines track the horizontal movement of the spray nozzles. B) Plot showing the optical thicknesses of **P1**/PEI films fabricated with ( $\bullet$ ) and without ( $\blacktriangle$ ) intermittent solvent rinse steps on silicon substrates versus the number of spray cycles (referred to as a 'bilayer'), as characterized by ellipsometry. Error bars represent the standard deviation of at least three measurements on three separate films. For some points, the error bars are smaller than the symbols used to represent the data and are thus not visible. The dotted (y = 5.5x,  $R^2 = 0.99$ ) and dashed (y = 16.9x,  $R^2 = 0.99$ ) lines are linear fits to the data forced through x = 0, y = 0.

the number of bilayers, consistent with stepwise, LbL growth and an average growth rate of  $\sim$ 5.5 nm for each bilayer. Subsequent experiments performed using longer spraying times ( $\sim$ 10 s) or with the addition of designated delay times of  $\sim$ 10 s between each spraying step yielded films with thicknesses and growth profiles that did not vary measurably from those shown in Figure 2B (data not shown), suggesting that processes that lead to film growth occur rapidly (e.g., with spray times as short as 6 s; we did not investigate spray cycles shorter than this in this study).

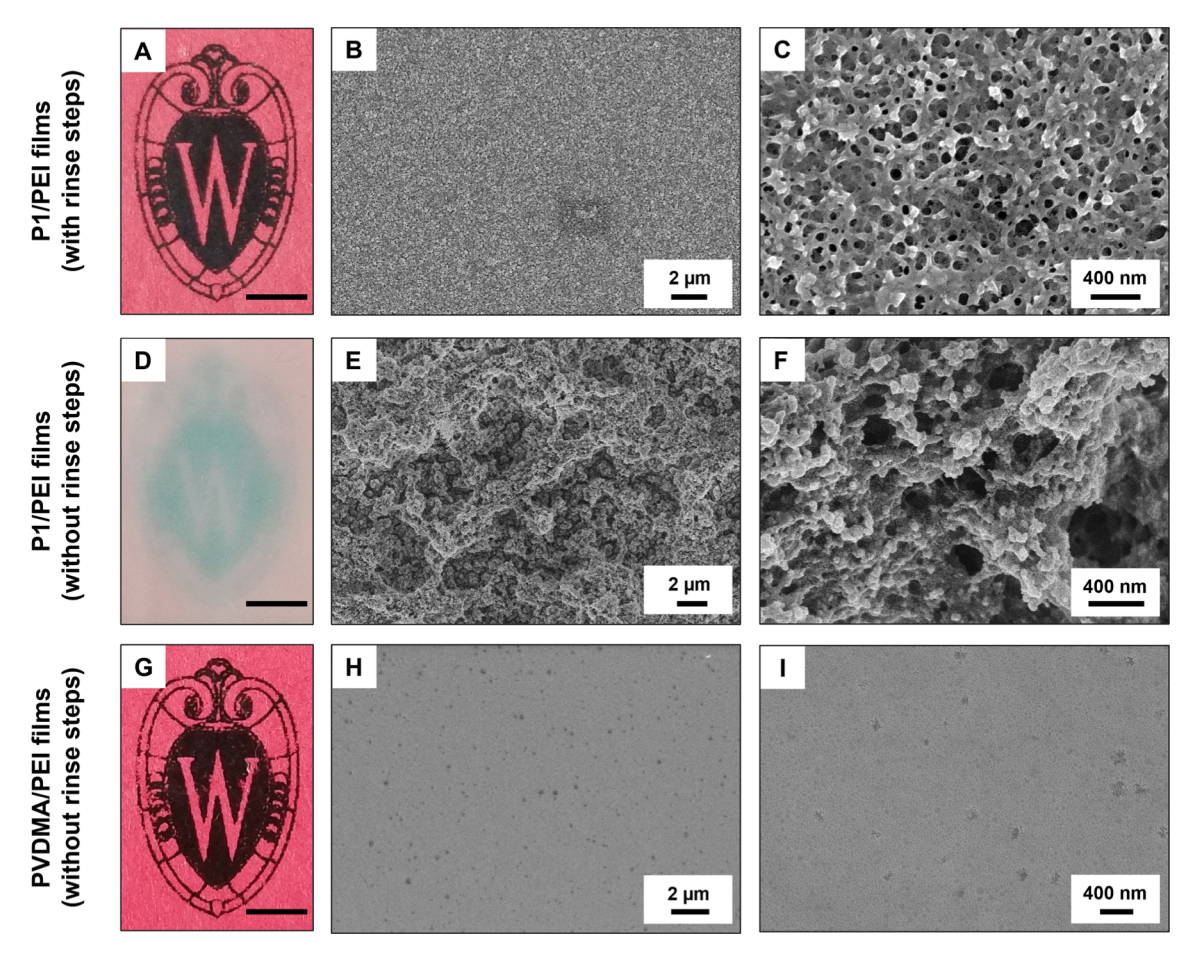


**Figure 3.** Digital photographs (A, D, G; scale bars = 25 mm) and low- and high-magnification top-down SEM images (B-C, E-F, H-I) of 35-bilayer **P1**/PEI films fabricated with (A-C) or without (D-F) rinse steps and 35-bilayer PVDMA/PEI films fabricated without (G-I) rinse steps. The digital photographs of film-coated glass substrates in panels A, D, and G were acquired with the substrate positioned over a printed red and black image used as a background; that image can be more clearly discerned in panels A and G. The crest logo shown in panels A, D, and G is used with permission granted by the University of Wisconsin–Madison.

Figure 3A shows a top-down photograph of a 35-bilayer P1/PEI film ~220 nm thick fabricated on a glass substrate. Inspection of this image reveals these films to be optically transparent, smooth, and uniform. Further characterization by SEM reveals coatings fabricated using this spray-based procedure to be relatively featureless and smooth on the micrometer scale and to exhibit nanometer-scale morphological features, including apparent surface nanoporosity (Figure 3B,C).

The solid curve in Figure 4A shows a representative PM-IRRAS spectrum of a P1/PEI coating fabricated on a gold-coated silicon substrate and reveals an absorbance peak at 1826 cm<sup>-1</sup> corresponding to the carbonyl group of the azlactone ring in P1. 13,36 Further inspection reveals a second peak centered at ~1670 cm<sup>-1</sup> that corresponds to two overlapping peaks that have been attributed in past studies<sup>13,36</sup> to (i) the amide I peak (C=O) corresponding to the amide bonds in P1 and those formed from the reaction of azlactone groups in P1 with primary amines in PEI and (ii) the peak corresponding to C=N functionality in the azlactone groups of P1. Overall, these and other results described below are consistent with an iterative, reactive spray-assembly process that leads to films that contain residual azlactone functionality at the surface and in the bulk of the material. Subsequent experiments demonstrated that these reactive spray-based coatings could be functionalized, post-fabrication, by treatment with amine-containing nucleophiles to modulate interfacial properties and pattern chemical functionality. The dashed curve in Figure 4A shows a representative PM-IRRAS spectrum of a P1/PEI film after treatment with a solution of the primary-amine-containing small molecule DMAPA. This result reveals the peak at 1826 cm<sup>-1</sup> to disappear, consistent with the exhaustive reaction of DMAPA with the unreacted azlactone groups in these materials and the installation of hydrophilic tertiary amine groups. Figure 4C-E demonstrates that this approach can be used to tailor the wetting behaviors of these spray-based coatings. The water contact angle of as-fabricated (azlactone-containing) films ( $\theta \approx 66^{\circ}$ , Figure 4C) decreased after treatment with hydrophilic DMAPA ( $\theta \approx 43^{\circ}$ , Figure 4D) and increased after treatment with the more hydrophobic nucleophile *n*-decylamine ( $\theta \approx 88^{\circ}$ , Figure 4E). We note that these coatings were physically stable (that is, they did not dissolve, erode, or delaminate from their underlying substrates) upon exposure to a range of organic

solvents, including THF and acetone used during functionalization steps, or upon immersion in aqueous solutions for several weeks.

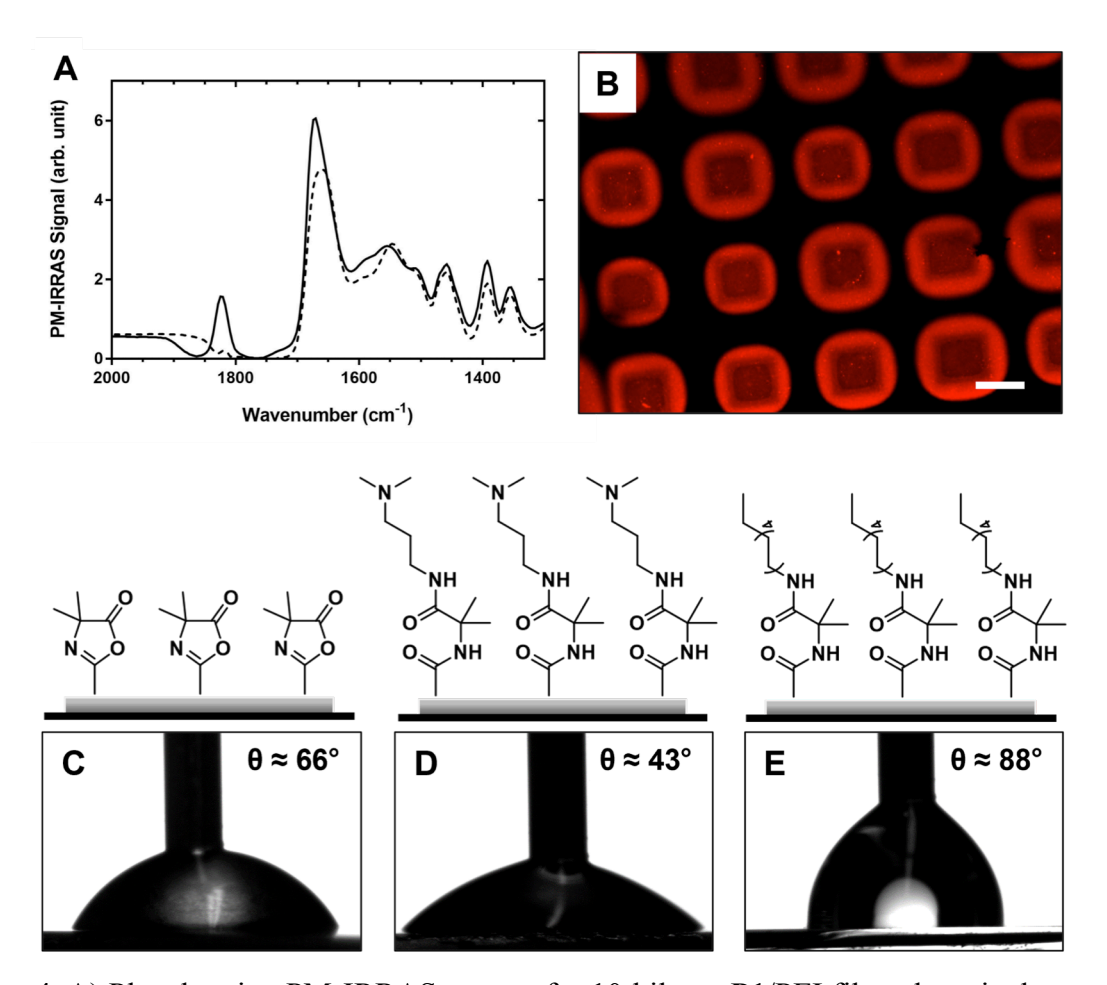


**Figure 4.** A) Plot showing PM-IRRAS spectra for 10-bilayer **P1**/PEI films deposited on a gold-coated silicon substrate before (solid line) and after (dashed line) functionalization by treatment with DMAPA overnight at room temperature. B) Fluorescence microscopy image of a native (azlactone-containing) **P1**/PEI film ~80 nm thick after reactive microcontact printing using a PDMS stamp and a solution of tetramethylrhodamine cadaverine. Scale bar =  $100 \mu m$ . C-E) Images showing contact angles of 5  $\mu$ L water droplets on 35-bilayer **P1**/PEI multilayers before (C) and after (D-E) functionalization with (D) DMAPA or (E) n-decylamine. The thickness of the needle used to dispense water as shown in the images is 0.718 mm. The accompanying schematic illustrations depict changes in the chemical structures of the films that occur upon treatment of the unreacted azlactone groups in these materials with primary amine-containing nucleophiles. For clarity, we note that these illustrations are not meant to indicate that functionalization occurs selectively at the surfaces of these coatings and that, for simplicity, residual amine functionality present in these films (see text) is not shown in these schematics.

P1/PEI film after reactive microcontact printing of the amine-containing fluorophore TMR-cad using a PDMS stamp patterned with 100-micron square posts (see Materials and Methods for additional details). The red fluorescent features in this image are consistent with covalent immobilization and patterning of TMR-cad on the film via reactions with residual azlactone groups. The intensity of these fluorescent features did not diminish after repeated rinsing with organic solvents, and otherwise identical control films pre-treated with propylamine to consume all remaining azlactone functionality prior to stamping showed no fluorescence (see Supporting Information, Figure S1), suggesting that the fluorescence observed in Figure 4B arises from covalent immobilization and not physisorption.

We used amine-based nucleophiles in the experiments described above because reactions between azlactones and primary amines generally occur rapidly and under mild conditions, <sup>39</sup> and this approach has also been used to functionalize a broad range of other azlactone-containing materials in past studies. <sup>40-47</sup> It is likely, based on the results above, that these spray-based coatings could also be functionalized with a range of thiol-containing, hydroxyl-containing, and other nucleophiles that react with azlactones under other conditions. <sup>39,48-50</sup> We also note that while the PVDMA/PEI films in this fundamental study were functionalized using over a period of hours, other recent studies from our group demonstrate that spray-based PVDMA/PEI films can be functionalized more rapidly (e.g., on the order of a minute) by passing the films through a continuous spray of solutions containing reactive amines. <sup>51</sup> Overall, we conclude on the basis of these initial studies that spray-based methods can be used to promote the LbL assembly using azlactone-containing polymers with retention of many of the salient features and practical

outcomes common for assemblies fabricated using immersion-based methods. The sections below describe approaches for tuning the physical and chemical morphologies and resulting behaviors of materials fabricated using spray-based methods in ways that are efficient and scalable and that would be difficult to achieve using immersion-based protocols.

Spray Assembly of Rough and Nanoporous Coatings: Characterization & Potential Applications

The results of additional experiments demonstrated that manipulation of spraying parameters, including the removal of solvent rinse steps between polymer spray steps, could bias P1/PEI film growth toward thicker films and result in the development of substantial nano- and microscale roughness and porosity. Figure 2B (solid triangles) shows a plot of optical thickness as a function of the number of P1/PEI spray cycles conducted in the absence of intermittent washing. These films also increased in thickness linearly, but at a significantly faster rate (~16 nm per bilayer) compared to films fabricated with intermittent rinse steps under otherwise identical conditions (~5.5 nm per bilayer; Figure 2A). After 10 bilayers, these coatings were ~190 nm thick; films fabricated by the application of additional spray cycles continued to grow (vide infra) but could no longer be characterized using ellipsometry because of substantial increases in roughness. Whereas films fabricated using spray cycles that included washing steps were smooth and optically transparent (Figure 3A shows a top-down image of a 35-bilayer thick film fabricated on a glass substrate, revealing the visual clarity of an underlying image), films fabricated in the absence of wash steps were optically opaque (Figure 3D) and exhibited surface roughness that was apparent to the naked eye. Further characterization of these coatings by SEM revealed micro-and nanoscale morphological features and multiscale, irregular porosity to be

present both on the surface (see top-down SEM images shown in Figure 3E, F) and throughout the bulk (see cross-sectional SEM images shown in Figure S2) of these films.

These rough and porous coatings also contained residual azlactone functionality, as indicted by the presence of an IR absorbance peak at 1826 cm<sup>-1</sup> (see Figure S3), and could be subsequently functionalized by treatment with small-molecule amines. The combination of surface topographic features and post-fabrication functionalization with hydrophilic and hydrophobic chemical functionality permitted the design of surface coatings that exhibited extreme wetting behaviors. For example, treatment of these thicker coatings (comprised of 35 P1/PEI bilayers) with solutions of DMAPA resulted in coatings that were superhydrophilic ( $\theta \approx$ 0°) and that, when submerged in water, were extremely non-wetting to liquid oils such as DCE (Figure 5A,B; small droplets of DCE (5 μL) exhibited an oil contact angle of ~160° on these surfaces, surpassing key criterion used to define so-called 'underwater superoleophobicity' 52,53). In contrast, treatment with *n*-decylamine yielded coatings that were superhydrophobic (e.g., a water contact angle of ~155°, with low water roll-off angles; 52,54 see Figure 5C-D and Video S1).

The roughness and porosity inherent to these superhydrophobic materials was sufficient to support the stable infusion of oily liquids, thus also rendering these 'no-wash' coatings useful for the design of slippery liquid-infused porous surfaces (SLIPS). Figure 6A-C shows top-down views of a glass substrate coated with decylamine-functionalized **P1**/PEI coatings infused with silicone oil. These time-lapse images also show a droplet of water (20  $\mu$ L; colored green to enhance visual contrast) sliding over the surface of the substrate (the substrate was tilted at 20°;

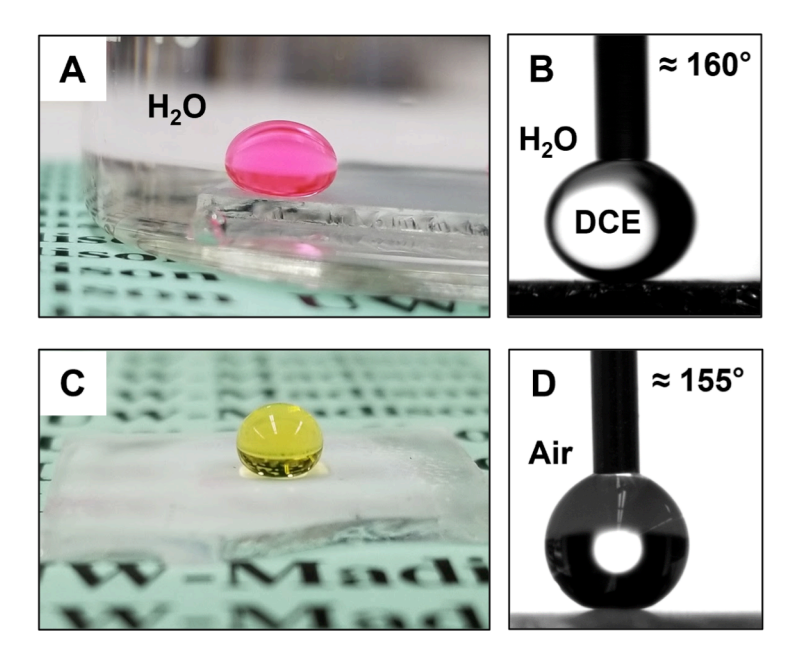


**Figure 5.** A,B) Representative images showing (A) beading of a droplet of DCE (colored red to aid visual observation) and (B) the static contact angle ( $\sim$ 160°) of DCE droplets on DMAPA-functionalized **P1**/PEI multilayers submerged under water. C,D) Images showing (C) beading of a droplet of water (colored green to aid visual observation) and (D) the static contact angle ( $\sim$ 155°) of water droplets, under air, on *n*-decylamine-functionalized **P1**/PEI multilayers. The thickness of the needle used to dispense water and DCE as shown in the images is 0.718 mm.

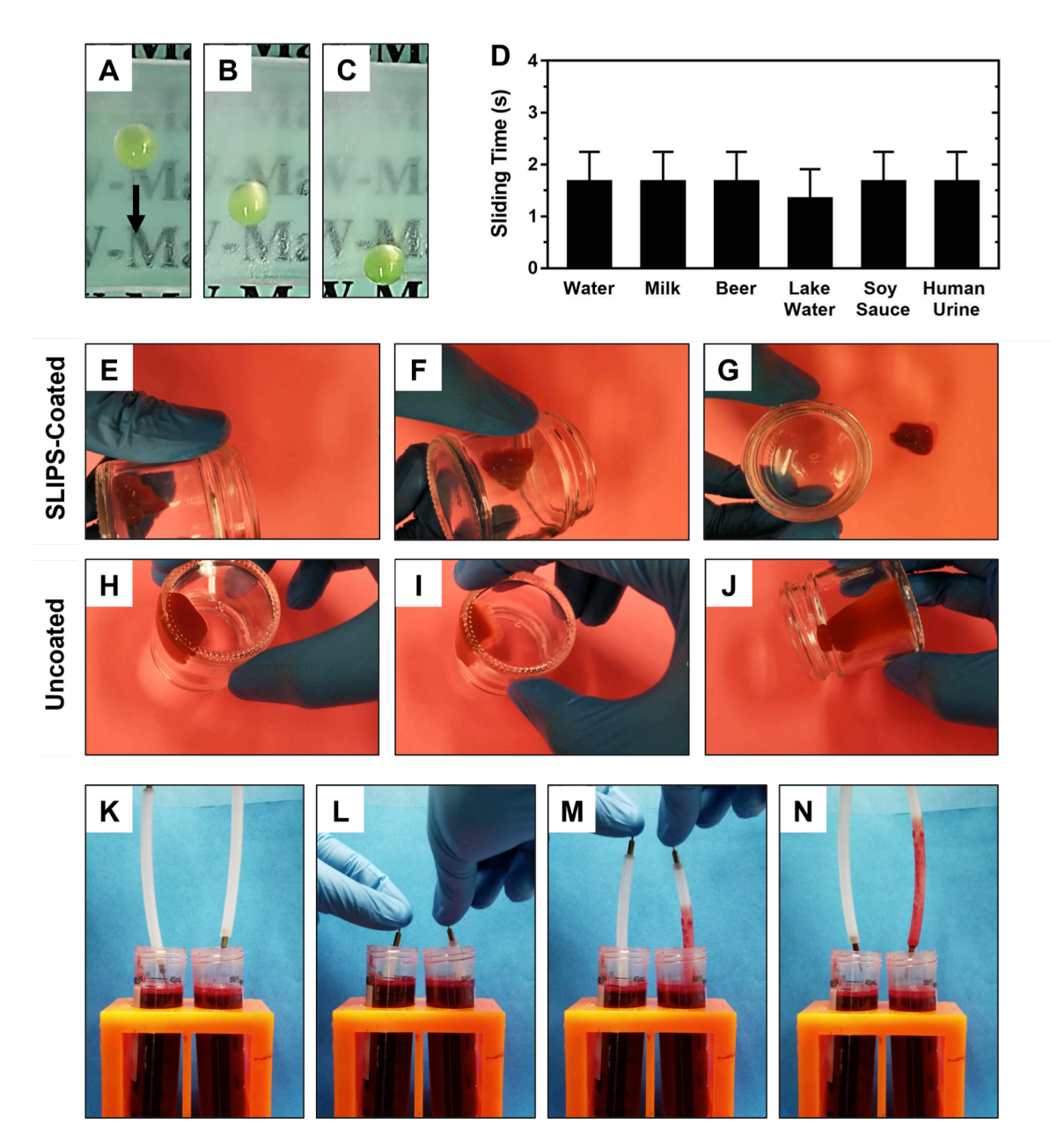


**Figure 6.** A-C) Top-down photographs showing a droplet of aqueous TMR (20 μL; tilt angle  $\approx$  20°) sliding on a glass substrate coated with a silicone oil-infused **P1**/PEI film (the glass slide is ~2 cm long). D) Plot showing the sliding times of different liquids on SLIPS-coated glass slides ~2 cm long; 20 μL droplets were used in each case and the substrates were tilted to 20°. E-G) Series of images showing a sample of tomato ketchup sliding around a SLIPS-coated glass container (see also Video S2). The glass container was spray-coated with a 35-bilayer **P1**/PEI coating that was then reacted with *n*-decylamine and infused with silicone oil prior to use. H-J) Series of images showing a sample of ketchup stuck inside a bare, uncoated glass container. K-N) Series of images showing that PE tubing segments (~ 8 cm long) dipped into whole blood (for ~10 s). In each panel, the tube on the left is coated with a **P1**/PEI SLIPS coating and the tube on the right is uncoated; see also Video S3).

the droplet was observed to slide at a rate of ~1 cm/s under these conditions). These SLIPS were stable and retained their slippery character upon contact with a range of chemically complex liquids, including milk, beer, lake water, soy sauce, and human urine, suggesting potential utility as non-fouling surfaces in a range of commercial and healthcare contexts (Figure 6D). The results of additional experiments showed that 'no-wash' coatings fabricated by spraying as few as 10 **P1**/PEI bilayers were sufficient to support infusion of oil and produce SLIPS, reducing the overall times needed to fabricate these anti-fouling materials by approximately one-third.

One potential practical advantage of the spray-based approach reported here is that it can be used to fabricate continuous and conformal coatings on objects of arbitrary shape or size. We used the protocol described above to fabricate a continuous SLIPS coating on the inside surface of a wide-mouthed glass container, used here as a small-scale model of a vessel useful for the storage and dispensing of commercial gels and liquids that would be difficult, cumbersome, or resource-intensive to coat using conventional immersion-based methods. Figure 6E-G shows selected images of a sample of tomato ketchup placed inside a SLIPS-coated container, and shows that the ketchup slid freely on the inside surfaces of the coated container (see also Video S2; images of a sample of ketchup in an uncoated container, which remained stuck to the walls of the container even at tilt angles of 90°, are included for comparison; see Figure 6H-J). We also used this sequential spray method to fabricate SLIPS coatings uniformly on the outside surfaces of lengths of flexible polyethylene (PE) tubing (see Figure S4 for additional details and discussion). Figure 6K-N shows a series of images of these SLIPS-coated tubes after contact with whole blood and reveals them to resist fouling in this context (in these images, SLIPScoated tubes are shown on the left side of each panel; uncoated control tubes are shown at right). Overall, these results highlight the potential of these spray-based methods to coat objects that would be otherwise unwieldy, time-consuming, expensive, or impractical to coat using dippingor flow-based methods.

Influence of Polymer Structure on Film Growth and Morphology

Additional experiments using PVDMA instead of P1 revealed the influence of side-chain hydrolysis (or the carboxylic acid group content) of P1 on structure formation during the fabrication of P1/PEI coatings. Both sequential and repetitive spraying of PVDMA (the unhydrolyzed reactive homopolymer from which P1 is synthesized; Figure 1) and PEI, without intermittent rinse steps, resulted in thin and optically transparent coatings (Figure 3G) that grew linearly to an average thickness of ~140 nm after 35 spray cycles. These PVDMA/PEI coatings were substantially thinner, both overall and on a per-bilayer basis, than 35-bilayer P1/PEI films fabricated under otherwise identical conditions (those films were ~1 µm thick, as determined from cross-sectional SEM images (Figure S2) and were optically opaque; Figure 3D). Additional characterization of these PVDMA/PEI coatings by SEM revealed them to be smooth and relatively featureless at both the micro-and nanoscale (Figure 3H, I), in contrast to films fabricated using P1 (Figure 3E, F).

These results, when combined, demonstrate that control over polymer (or copolymer) structure can be exploited in the context of spray-based assembly to obtain morphologies, properties, and behaviors that are desirable and useful in the context of particular potential applications. The mechanisms underlying the evolution of roughness and porosity in these systems are not completely understood. These results are, however, consistent with those of past studies on immersion-based assembly demonstrating the role that strategic levels of side chain hydrolysis can play in biasing film growth and morphology in PVDMA/PEI films, including the

evolution of nano/microscale roughness and porosity, which was suggested to occur via additional acid/base, ionic, or hydrogen-bonding interactions between **P1** and PEI promoted by the ionizable carboxylate side chains of **P1** during assembly).<sup>36</sup>

Overall, the results summarized in Figure 3 and discussed above demonstrate that both polymer structure (e.g., side chain hydrolysis) and process parameters (e.g., the presence or absence of intermittent wash steps) can be manipulated to design films with a broad range of useful properties. In addition to providing useful control over film architecture and function, the elimination of intermittent rinse steps also substantially reduces overall coating times by as much as one-third compared to protocols involving solvent rinses. We note that the spray-based procedures reported here also permit fabrication of azlactone-containing coatings using nonpolymeric amine-containing building blocks, leading to materials with significantly different architectures and properties compared to P1/PEI assemblies. The results of experiments to fabricate and characterize reactive, spray-based coatings using (i) small-molecule (nonpolymeric) diamine linkers and (ii) amine-functionalized nanoparticles are included as Supplementary Information (see Figures S5 and S6). Further manipulation of other process parameters (e.g., spray angle and droplet size, spraying rate, and incorporation of additional intermittent rinsing or drying steps) are likely to also lead to new physical and chemical behaviors and have the potential to further improve manufacturing efficiency or broaden the range of potential applications for which these reactive coatings could be useful.

## Fabrication of Reactive Coatings by Simultaneous Spray Assembly

Subsequent experiments demonstrated that coatings with useful features could also be fabricated by spraying P1 and PEI as reactive building blocks simultaneously (i.e., at the same

time, continuously, and with no washing steps; see schematic in Figure 7A). To explore the feasibility of this approach, we simultaneously sprayed dilute solutions of **P1** and PEI at five different **P1**/PEI spray rate ratios (1:7, 1:3, 1:1, 1.9:1, and 3:1, achieved by spraying different concentrations of P1 and PEI solutions at the same flow rates) while keeping the combined polymer spraying rate  $(7.2 \pm 1.2 \text{ mmol/s})$  constant. For these experiments, all other film fabrication parameters, including spray volume, spray angle, and spray distance, were maintained as described above for alternating LbL-based spraying procedures (see Materials and Methods for additional details) and coatings were deposited on silicon substrates to facilitate characterization of film thicknesses and growth.

Figure 7B shows a plot of optical thickness as a function of spraying time for these different P1/PEI spray rate ratios. The dotted lines represent fitted linear regression curves ( $R^2 \ge 0.99$ ) to these measured optical thicknesses, and reveal film thickness to increase linearly as a function of continuous spraying time regardless of the P1/PEI spray rate ratio used. Due to the notably increased opacity of films fabricated at the 1:1 P1/PEI ratio at longer spray times, thicknesses could not be measured by ellipsometry. We therefore estimated the thicknesses of films fabricated at this condition (e.g., a 1:1 P1/PEI ratio after spraying for 145 s) from cross-sectional SEM images (see Figure S7; the thickness value resulting from this measurement is indicated by the red triangle in Figure 7B, which is also marked with an asterisk to differentiate it from values obtained using ellipsometry). We caution that this SEM-derived thickness cannot be compared formally to the optical thicknesses measured using ellipsometry. We note, however, that this physical thickness falls near a value close to what would be predicted based on the linear growth rate observed during shorter spraying times (Figure 7B, filled inverted triangles; the dashed arrow shows a linear projection to longer times and is included only to guide the eye).

Overall, we found the P1/PEI spray ratio to influence film growth rate, with maximum growth rates observed for the continuous spraying at a ratio of 1:1 (Figure 7B; Figure 7C also

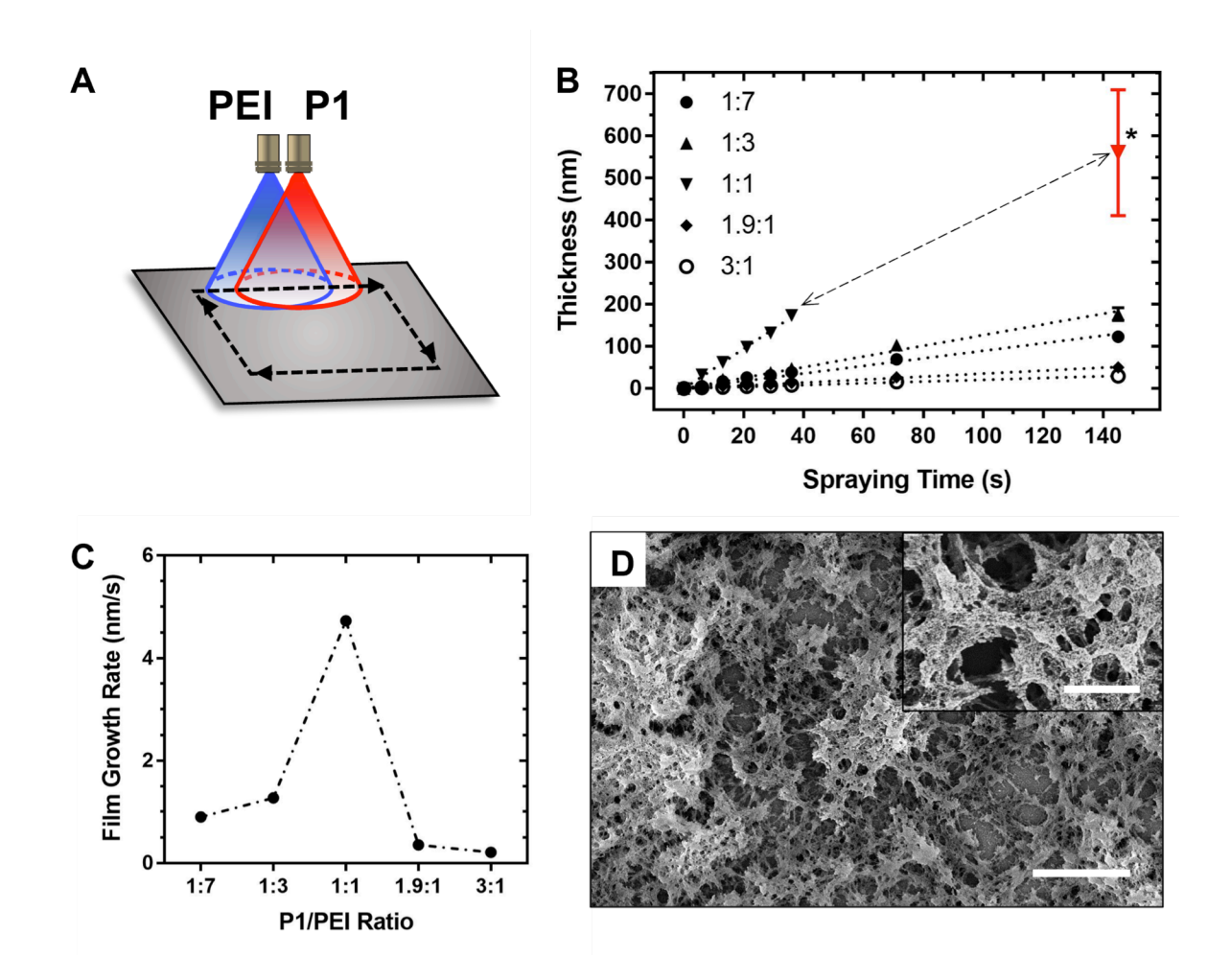


Figure 7. A) Schematic showing the simultaneous spraying of P1 and PEI to fabricate P1/PEI coatings. The dotted lines track the horizontal movement of the spray nozzles. B) Plot showing the optical thicknesses of P1/PEI films, as characterized by ellipsometry, as a function of number of cumulative spraying time at five different ratios of spraying rates, 1:7 (•), 1:3 (•), 1:1 (•), 1.9:1 (•), and 3:1 (•). The combined P1 and PEI spraying rate was kept constant at  $7.2 \pm 1.2$  mmol/s (see text). For some points, the error bars are smaller than the sizes of the symbols used to represent the data and are therefore not visible. For the 1:1 P1/PEI ratio, the thickness after 145 s of spraying time (denoted in the plot by a red-colored inverted triangle with an asterisk;  $\checkmark$ \*) was determined from cross-sectional SEM images (see Figure S7 and additional discussion in the text). The dotted lines are the linear fits ( $R^2 \ge 0.99$ ) to the data forced through x=0 and y=0. The dashed double arrow is included only as a guide to the eye (see text). C) Plot showing the growth rate (taken from the slopes of the dotted lines shown in (B) versus the P1/PEI spraying rate ratio; error bars are smaller than the sizes of the symbols used to represent the data. D) Low- and high-magnification (inset) SEM images of coatings fabricated by simultaneously spraying P1 and PEI at 1:1 ratio of spraying rates on a silicon substrate for 145 seconds. Scale bar = 2  $\mu$ m; 400 nm insets.

shows a plot of the growth rates, determined from the slopes of linear regression curves in Figure 7B, as a function of P1/PEI spray rate ratios). Film growth rates decreased substantially when spray rate ratios deviated from 1:1. For example, whereas films fabricated with a P1/PEI spray rate ratio of 1:1 were ~560 nm thick after 145 s of spraying, coatings fabricated using ratios of 1:7, 1:3, 1.9:1, and 3:1 reached thicknesses of ~135 nm, ~100 nm, ~40 nm, and ~10 nm, respectively, after 145 s of spraying. All films fabricated by simultaneously spraying P1 and PEI exhibited roughness that was visible to the naked eye under all conditions tested. Figure 7D shows a representative top-down SEM image of a film fabricated using a 1:1 spray rate ratio. This coating appears to have a rough and granular morphology that consists of micro-and nanoscale aggregates. This granular or irregular microscale morphology was also observed for simultaneously sprayed films fabricated at other spray rate ratios (see Figure S8). Characterization of films that were scratched prior to imaging revealed an ultrathin continuous polymer film covering the silicon substrates and surrounding the salient micro-and nanoscale features in these images (see Figure S9 and insets in Figure S8). Overall, the morphologies of these simultaneously sprayed films varied significantly from those observed for sequentially sprayed films described above (as shown in Figure 7D and Figure 3E-F).

The results above are consistent with a mechanism of film growth that involves the continuous formation and deposition of polymer aggregates during simultaneous spraying. General support for this view is provided by observations of large and visible aggregates that form within several seconds when solutions of PEI and P1 are mixed as a result of reactions between amines and azlactone groups and other ion-pairing interactions with PEI that could arise from the presence of carboxylic acid side chains.<sup>36</sup> During simultaneous spraying, aggregates or complexes of these polymers are likely to form continuously and either (i) drain from the surface

under forced flow or (ii) deposit on the surface continuously during fabrication in ways that depend upon the ratio of the two polymers in the mixture (similar to behaviors described previously for aggregates formed during the simultaneous spraying of oppositely charged polyelectrolytes<sup>30,32,58,59</sup>). In the case of both low and high P1/PEI ratios, where an excess of either P1 or PEI is present, we speculate that the likelihood of the deposition of aggregates on the surface would be smaller compared to aggregates formed when P1 and PEI are sprayed at ratios close to 1:1. At these conditions, aggregates formed in solution would be more likely to drain from the surface (due to an excess of amine or azlactone functionality in the aggregate), leading to reduced film growth, consistent with results shown in Figure 7B-C. In any case, continuous spraying appears to result in the continuous formation and deposition of polymer complexes, resulting in gradual film growth over time (as observed by the linear increases in the film thickness shown in Figure 7B; see also Figure S10 for SEM images of P1/PEI coatings at different spraying times, which reveal an increase in overall film coverage and other changes in morphology as a function of spray time). These results also suggest opportunities to manipulate process parameters in ways that permit the microscale morphologies, and thus the functional properties, of these coatings to be further tuned (e.g., such as wetting behavior; Figure S11 shows changes in water contact angles that can be achieved by manipulation of spraying rate ratios). Finally, we note that structure formation in these simultaneously sprayed materials can again be influenced by side-chain azlactone hydrolysis. In general, films formed using unhydrolyzed PVDMA were visually smooth and transparent (see Figure S12A,C) and lacked larger micron-scale features and porosity apparent in simultaneously sprayed P1/PEI films (see Figure S12B-D).

## Reactive Functionalization and Characterization of Simultaneously Sprayed Coatings

We conducted a final series of experiments to characterize the reactivities and functional properties of the thicker **P1**/PEI films described above fabricated using simultaneous spraying and a spray rate ratio of 1:1. Figure 8A (solid curve) shows a representative IR spectrum for a simultaneously sprayed film fabricated on a gold-coated silicon substrate and again shows (i) an absorbance peak at 1826 cm<sup>-1</sup> corresponding to the carbonyl group of the unreacted azlactone functionality and (ii) a peak at ~1670 cm<sup>-1</sup> characteristic of amide bonds that form when PVDMA reacts with primary amines. Exposure of these films to *n*-decylamine at room temperature (see the dotted curve in Figure 8A) results in a significant decrease in the peak at 1826 cm<sup>-1</sup> and increases in the amide I peak at 1670 cm<sup>-1</sup> and a distinct amide II peak at 1544 cm<sup>-1</sup>. These results, when combined with the stability of these films upon extended exposure to organic solvents, are consistent with covalent crosslinking and demonstrate that simultaneous spraying leads to coatings that retain residual azlactone functionality that is available for further reaction and post-fabrication manipulation of film features.

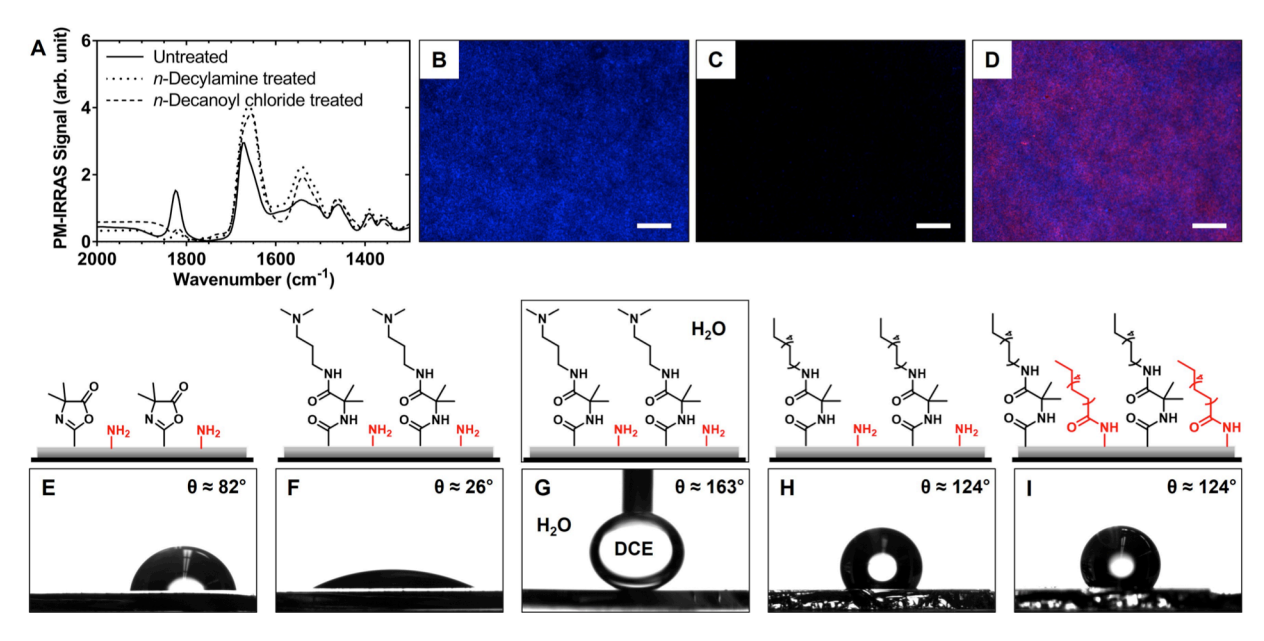


Figure 8. A) Plot showing PM-IRRAS spectra for P1/PEI films (fabricated using simultaneous spraying-based procedures, P1/PEI spraying ratio = 1:1) deposited on a gold-coated silicon substrate before functionalization (solid line) and after treatment with n-decylamine (dotted line) and then treatment with *n*-decanoyl chloride (dashed line; refer to the main text for more details). B,C) Fluorescence microscopy images of a (B) amine-containing (C) decanoyl chloride-treated P1/PEI film (~170 nm thick, fabricated on a silicon substrates, and pretreated with propylamine to exhaust residual azlactone functionality) after treatment with 7-(diethylamino)coumarin-3-carboxylic acid N-succinimidyl ester. (D) Merged fluorescence images of native (amine and azlactone-containing) P1/PEI films after treatment with tetramethylrhodamine cadaverine, followed by treatment with coumarin-NHS ester. Scale bars = 100  $\mu$ m. E-I) Images showing contact angles of 5  $\mu$ L water droplets on P1/PEI films (E) before and after (F-I) functionalization with (F) DMAPA (the contact angle of a 5 µL DCE droplet on the same film under water is shown in (G)), (H) n-decylamine, and (I) n-decylamine followed by *n*-decanoyl chloride. The thickness of the needle used to dispense water as shown in panel G is 0.718 mm. The accompanying schematic illustrations depict changes in the chemical structures of the films that occur upon treatment of the unreacted azlactone and amine groups in these materials with primary amines or acid chlorides, respectively. For clarity, we note that these illustrations are not meant to indicate that functionalization occurs selectively at the surfaces of these coatings.

Additional experiments demonstrated that residual amine-based chemical functionality associated with PEI can also be chemically modified, post-fabrication, with a range of amine-reactive electrophiles, including compounds containing N-succinimidyl esters and chloroformyl groups. Figure 8B shows an image of a film ( $\sim$ 170 nm thick and pre-treated, in the manner described above, with n-propylamine to exhaust remaining azlactone functionality) that was

treated with a solution of an amine-reactive fluorophore (7-(diethylamino)coumarin-3-carboxylic acid N-succinimidyl ester). This image clearly shows the presence of fluorescence (false-colored blue) throughout the film. Figure 8C shows the result of an otherwise identical experiment using a **P1**/PEI film that was first treated with propionyl chloride to exhaust residual amine functionality prior to treatment with the N-succinimidyl fluorophore. Taken together, these results suggest that the fluorescence observed in Figure 8B is the result of the covalent reaction of the fluorophore with the residual amine functionality in these materials (e.g., as opposed to physisorption). Spectroscopic characterization of the reaction of the amines in these films with acyl chlorides or other electrophiles was complicated by the existing amide I peak at  $\sim 1650$  cm<sup>-1</sup> in these materials (Figure 8A, dashed line). However, the results of these fluorescence microscopy experiments and changes in the functional properties of these coatings upon treatment with amine-reactive molecules (described below) demonstrate that these azlactone-containing **P1**/PEI films can also be modified, post-fabrication, by treatment with a range of amine-reactive electrophiles.

The presence of both amine and azlactone functionality in these films creates opportunities to immobilize molecules containing both nucleophilic and electrophilic functional groups on these surfaces. Figure 8D shows a merged fluorescence image of a film treated with an amine-functionalized fluorophore (tetramethylrhodamine cadaverine, false-colored red) followed by treatment with the N-succinimidyl ester-functionalized fluorophore described above (false-colored blue). It is also possible to exploit this dual functionality to tailor the physical properties (e.g., the wetting behaviors) of surfaces coated with these reactive films by treatment with combinations of reactive hydrophilic and hydrophobic molecules. For example, treatment of P1/PEI films with solutions of DMAPA resulted in significantly hydrophilic coatings ( $\theta \approx 26^{\circ}$ ,

compared to the untreated films ( $\theta \approx 82^\circ$ ); Figure 8E-F) and, when submerged in water, these DMAPA-treated films exhibited underwater superoleophobicity (Figure 8G;  $\theta \approx 163^\circ$ ). In contrast, treatment with *n*-decylamine resulted in a significant increase in the water contact angles of these films ( $\theta \approx 124^\circ$ , Figure 8H). These *n*-decylamine-treated films did not, however, exhibit robust slippery characteristics when infused with silicone oil (in general, these surfaces became less slippery, as determined by characterization of the sliding times of liquid droplets on these surfaces after a few minutes of immersion in, and subsequent removal from, water). However, when we further reacted these decylamine-treated films with decanoyl chloride to react with residual amine functionality ( $\theta \approx 124^\circ$ , Figure 8I) and then infused the films with silicone oil, the resulting slippery surfaces ( $\theta_{hys} \approx 5^\circ$ ) remained stable under a range of conditions and upon subjection to a range of subsequent physical and chemical insults (as described below).

Figure 9 reveals these oil-infused, dual-functionalized coatings to remain stable and slippery when contacted with a range of chemically complex liquids (panel A) and to retain their anti-fouling properties upon repeated bending and flexing (panels B-E), deep scratching (F-H), or permanent creasing (panels I-K) of the coatings or the underlying substrates. These features reflect the soft and flexible nature of the coatings themselves, and allow these materials to either

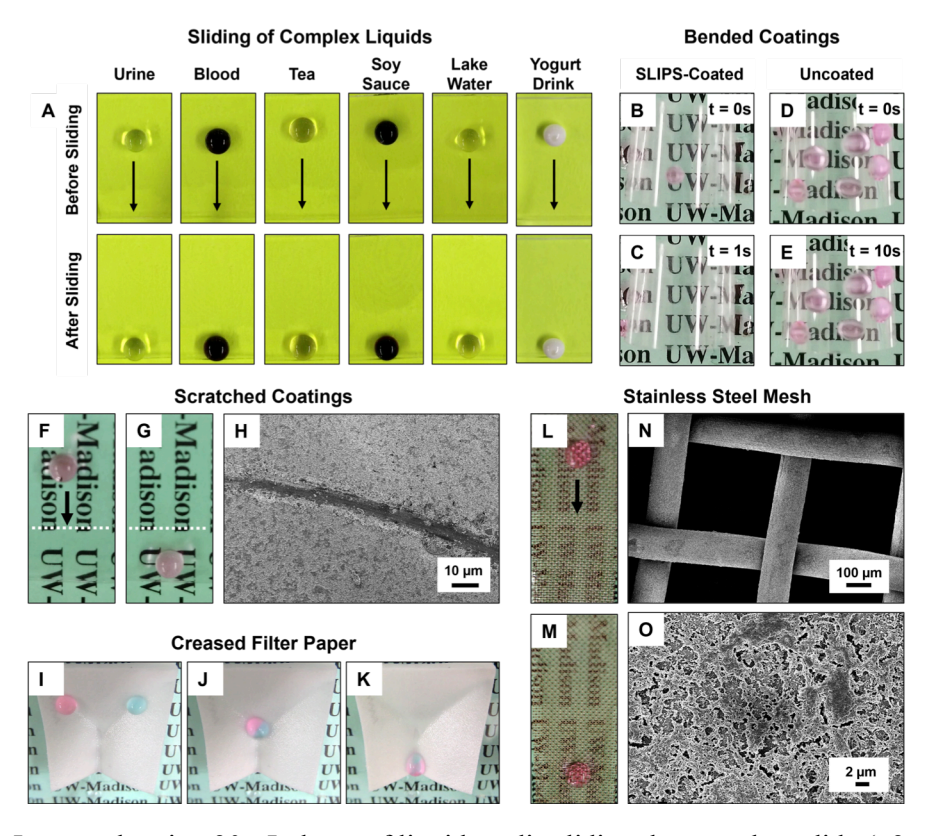


**Figure 9.** A) Images showing 20 μL drops of liquid media sliding down a glass slide (~2 cm long, tilted to  $20^{\circ}$ ) coated with silicone oil-infused **P1**/PEI films: droplets of urine, blood, tea, soy sauce, eutrophic lake water and yogurt drink are shown. See also Video S4. (B-E) Top-down perspective showing droplets of aqueous TMR (20 μL) on a sample of SLIPS-coated (B,C) and uncoated (D,E) flexible polyester substrates bent and held end-to-end. See also Video S5. (F,G) Photographs showing the sliding of a droplet of aqueous TMR on a SLIPS-coated glass substrate (~2 cm long) that was scratched in multiple locations (marked by the dotted white line); the droplet was observed to slide unperturbed over the scratches. (H) SEM image of the scratched coating showing the scratched region; this image was acquired after leaching of the infused oil phase. (I-K) Images showing the sliding of aqueous droplets (15 μL; colored red and blue to aid visual observation) on SLIPS-coated filter paper. SLIPS coated filter paper was permanently creased prior to placing the aqueous droplets, and the aqueous droplets were observed to slide on the crease. See also Video S6. L,M) A droplet of aqueous TMR (20 μL) sliding on SLIPS-coated stainless-steel wire mesh. N,O) Low- and high magnification SEM images of **P1**/PEI coatings on wire mesh prior to oil infusion.

(i) survive physical forces and manipulation associated with many potential applications of these materials or (ii) be bent, folded, or manipulated, post-fabrication, into new geometries or other designs required for specific potential applications. Finally, the simultaneous spray-based procedures reported here are appropriate for fabricating functional coatings and anti-fouling SLIPS on surfaces with topologically complex features. Panels L-O of Figure 9 show rough and nanoporous P1/PEI coatings sprayed onto stainless-steel wire meshes and the sliding behaviors of droplets of water on the surfaces of coated meshes infused with silicone oil. Our results reveal these sprayed coatings to cover the surfaces of these topographically complex substrates uniformly and conformally.

## **Summary and Conclusions**

We have reported new alternating LbL and continuous/simultaneous spray-based approaches to the assembly of soft material coatings fabricated using azlactone-containing polymers and amine-containing building blocks. Our results reveal several important ways in which polymer structure (e.g., the presence or absence of hydrolyzed azlactone groups) and spray-process parameters (e.g., the number of spray cycles, the elimination of intermittent wash cycles, or the manipulation of polymer solution spray rates) can influence aspects of film growth and morphology that impart properties relevant to several potential applications of these materials. Judicious manipulation of these parameters—or combinations of these parameters—permits rapid deposition of reactive coatings that are either thin and optically transparent or thicker and optically opaque, with varying levels of nano- and microscale roughness or porosity. These spray-based coatings can be further functionalized, post-fabrication, by treatment with amine-based nucleophiles and/or electrophilic amine-reactive species to impart new chemical

functionality, providing means to tune the interfacial (e.g., wetting) properties of these coatings, pattern new surface features, or create porous coatings useful for the design of new types of antifouling oil-infused surfaces. These spray-based methods can be applied using automated processes that are well-suited for the coating of large objects and are faster and more amenable to scale-up and adoption in the context of continuous manufacturing than previously reported LbL methods that involve the repeated immersion of objects into polymer baths. Overall, the results reported here provide new methods and fundamental insights useful for tuning and tailoring the properties and behaviors of azlactone-containing materials, surfaces, and interfaces. 40-47 We anticipate that these spray-based methods will help guide the development of new processes for the fabrication of these reactive coatings that can be implemented at scale or as elements of commercial or industrial processes. 51

**Acknowledgments.** Financial support for this work was provided in part by the National Science Foundation through a grant provided to the UW–Madison Materials Research Science and Engineering Center (MRSEC; DMR-1720415), and by the UW-Madison Wisconsin Alumni Research Foundation (WARF) through grants provided by the WARF Accelerator Program and the Draper Technology Innovation Fund (Draper-TIF). The authors acknowledge the use of instrumentation supported by the NSF through the UW MRSEC (DMR-1720415).

**Supporting Information.** Images, plots, and videos containing additional physical, chemical, and functional characterization of dry and oil-infused spray coatings (PDF). This material is available free of charge via the Internet.

## ORCID

David M. Lynn: 0000-0002-3140-8637

## References

- Multilayer Thin Films: Sequential Assembly of Nanocomposites Materials, 2nd ed.; Decher,
  G.; Schlenoff, J. B., Eds.; Wiley-VCH, 2012.
- 2. Layer-by-Layer Films for Biomedical Applications, Picart, C.; Caruso, F.; Voegel, J. C., Eds.; Wiley-VCH, 2015.
- 3. Schönhoff, M. Self-Assembled Polyelectrolyte Multilayers. *Curr. Opin. Colloid Interface Sci.* **2003**, *8*, 86-95.
- 4. Borges, J.; Mano, J. F. Molecular Interactions Driving the Layer-by-Layer Assembly of Multilayers. *Chem. Rev.* **2014**, *114*, 8883-8942.
- 5. Yuan, W.; Weng, G.-M.; Lipton, J.; Li, C. M.; Van Tassel, P. R.; Taylor, A. D. Weak Polyelectrolyte-Based Multilayers via Layer-by-Layer Assembly: Approaches, Properties, and Applications. *Adv. Colloid Interface Sci.* **2020**, *282*, 102200.
- 6. Guzmán, E.; Rubio, R. G.; Ortega, F. A Closer Physico-Chemical Look to the Layer-by-Layer Electrostatic Self-Assembly of Polyelectrolyte Multilayers. *Adv. Colloid Interface Sci.* **2020**, *282*, 102197.
- 7. Quinn, J. F.; Johnston, A. P. R.; Such, G. K.; Zelikin, A. N.; Caruso, F. Next Generation, Sequentially Assembled Ultrathin Films: Beyond Electrostatics. *Chem. Soc. Rev.* **2007**, *36*, 707-718.
- 8. Broderick, A. H.; Lynn, D. M., Covalent Layer-by-Layer Assembly Using Reactive Polymers. In *Functional Polymers by Post-Polymerization Modification: Concepts*,

- *Practical Guidelines, and Applications*, Theato, P.; Klok, H. A., Eds. Wiley-VCH: 2012; pp. 371-406.
- 9. Bergbreiter, D. E.; Liao, K.-S. Covalent Layer-by-Layer Assembly—An Effective, Forgiving Way to Construct Functional Robust Ultrathin Films and Nanocomposites. *Soft Matter* **2009**, *5*, 23-28.
- Rydzek, G.; Schaaf, P.; Voegel, J.-C.; Jierry, L.; Boulmedais, F. Strategies for Covalently Reticulated Polymer Multilayers. *Soft Matter* 2012, 8, 9738-9755.
- 11. An, Q.; Huang, T.; Shi, F. Covalent Layer-by-Layer Films: Chemistry, Design, and Multidisciplinary Applications. *Chem. Soc. Rev.* **2018**, *47*, 5061-5098.
- 12. Xiao, F.-X.; Pagliaro, M.; Xu, Y.-J.; Liu, B. Layer-by-Layer Assembly of Versatile Nanoarchitectures with Diverse Dimensionality: A New Perspective for Rational Construction of Multilayer Assemblies. *Chem. Soc. Rev.* **2016**, *45*, 3088-3121.
- Buck, M. E.; Zhang, J.; Lynn, D. M. Layer-by-Layer Assembly of Reactive Ultrathin Films Mediated by Click-Type Reactions of Poly(2-Alkenyl Azlactone)s. *Adv. Mater.* 2007, 19, 3951-3955.
- 14. Broderick, A. H.; Azarin, S. M.; Buck, M. E.; Palecek, S. P.; Lynn, D. M. Fabrication and Selective Functionalization of Amine-Reactive Polymer Multilayers on Topographically Patterned Microwell Cell Culture Arrays. *Biomacromolecules* 2011, 12, 1998-2007.
- 15. Broderick, A. H.; Carter, M. C. D.; Lockett, M. R.; Smith, L. M.; Lynn, D. M. Fabrication of Oligonucleotide and Protein Arrays on Rigid and Flexible Substrates Coated with Reactive Polymer Multilayers. *ACS Appl. Mater. Interfaces* **2013**, *5*, 351-359.

- Buck, M. E.; Schwartz, S. C.; Lynn, D. M. Superhydrophobic Thin Films Fabricated by Reactive Layer-by-Layer Assembly of Azlactone-Functionalized Polymers. *Chem. Mater.* 2010, 22, 6319-6327.
- 17. Manna, U.; Lynn, D. M. Synthetic Surfaces with Robust and Tunable Underwater Superoleophobicity. *Adv. Funct. Mater.* **2015**, *25*, 1672-1681.
- Manna, U.; Lynn, D. M. Fabrication of Liquid-Infused Surfaces Using Reactive Polymer Multilayers: Principles for Manipulating the Behaviors and Mobilities of Aqueous Fluids on Slippery Liquid Interfaces. *Adv. Mater.* 2015, 27, 3007-3012.
- 19. Hammond, P. T. Engineering Materials Layer-by-Layer: Challenges and Opportunities in Multilayer Assembly. *AlChE J.* **2011**, *57*, 2928-2940.
- 20. Richardson, J. J.; Björnmalm, M.; Caruso, F. Technology-Driven Layer-by-Layer Assembly of Nanofilms. *Science* **2015**, *348*, aaa2491.
- 21. Richardson, J. J.; Cui, J.; Björnmalm, M.; Braunger, J. A.; Ejima, H.; Caruso, F. Innovation in Layer-by-Layer Assembly. *Chem. Rev.* **2016**, *116*, 14828-14867.
- 22. Schlenoff, J. B.; Dubas, S. T.; Farhat, T. Sprayed Polyelectrolyte Multilayers. *Langmuir* **2000**, *16*, 9968-9969.
- 23. Li, Y.; Wang, X.; Sun, J. Layer-by-Layer Assembly for Rapid Fabrication of Thick Polymeric Films. *Chem. Soc. Rev.* **2012**, *41*, 5998-6009.
- 24. Dierendonck, M.; De Koker, S.; De Rycke, R.; De Geest, B. G. Just Spray It LbL Assembly Enters a New Age. *Soft Matter* **2014**, *10*, 804-807.
- 25. Izquierdo, A.; Ono, S. S.; Voegel, J. C.; Schaaf, P.; Decher, G. Dipping Versus Spraying: Exploring the Deposition Conditions for Speeding up Layer-by-Layer Assembly. *Langmuir* 2005, 21, 7558-7567.

- 26. Krogman, K. C.; Lowery, J. L.; Zacharia, N. S.; Rutledge, G. C.; Hammond, P. T. Spraying Asymmetry into Functional Membranes Layer-by-Layer. *Nat. Mater.* **2009**, *8*, 512-518.
- 27. Kyung, K.-H.; Shiratori, S. Nanoscale Texture Control of Polyelectrolyte Multilayer Using Spray Layer-by-Layer Method. *Jpn. J. Appl. Phys.* **2011**, *50*, 025602.
- 28. Mulhearn, W. D.; Kim, D. D.; Gu, Y.; Lee, D. Facilitated Transport Enhances Spray Layer-by-Layer Assembly of Oppositely Charged Nanoparticles. *Soft Matter* **2012**, *8*, 10419-10427.
- 29. Alongi, J.; Carosio, F.; Frache, A.; Malucelli, G. Layer by Layer Coatings Assembled through Dipping, Vertical or Horizontal Spray for Cotton Flame Retardancy. *Carbohydr. Polym.* **2013**, *92*, 114-119.
- 30. Porcel, C. H.; Izquierdo, A.; Ball, V.; Decher, G.; Voegel, J. C.; Schaaf, P. Ultrathin Coatings and (Poly(Glutamic Acid)/Polyallylamine) Films Deposited by Continuous and Simultaneous Spraying. *Langmuir* **2005**, *21*, 800-802.
- 31. Lefort, M.; Popa, G.; Seyrek, E.; Szamocki, R.; Felix, O.; Hemmerlé, J.; Vidal, L.; Voegel, J.-C.; Boulmedais, F.; Decher, G.; Schaaf, P. Spray-On Organic/Inorganic Films: A General Method for the Formation of Functional Nano- to Microscale Coatings. *Angew. Chem. Int. Ed.* 2010, 49, 10110-10113.
- 32. Schaaf, P.; Voegel, J.-C.; Jierry, L.; Boulmedais, F. Spray-Assisted Polyelectrolyte Multilayer Buildup: From Step-by-Step to Single-Step Polyelectrolyte Film Constructions. *Adv. Mater.* **2012**, *24*, 1001-1016.
- 33. Chen, Q.; Brett, C. J.; Chumakov, A.; Gensch, M.; Schwartzkopf, M.; Körstgens, V.; Söderberg, L. D.; Plech, A.; Zhang, P.; Müller-Buschbaum, P.; Roth, S. V. Layer-by-

- Layer Spray-Coating of Cellulose Nanofibrils and Silver Nanoparticles for Hydrophilic Interfaces. *ACS Applied Nano Materials* **2021,** *4*, 503-513.
- 34. Brett, C. J.; Mittal, N.; Ohm, W.; Gensch, M.; Kreuzer, L. P.; Körstgens, V.; Månsson, M.; Frielinghaus, H.; Müller-Buschbaum, P.; Söderberg, L. D.; Roth, S. V. Water-Induced Structural Rearrangements on the Nanoscale in Ultrathin Nanocellulose Films. *Macromolecules* 2019, 52, 4721-4728.
- 35. Buck, M. E.; Lynn, D. M. Functionalization of Fibers Using Azlactone-Containing Polymers: Layer-by-Layer Fabrication of Reactive Thin Films on the Surfaces of Hair and Cellulose-Based Materials. *ACS Appl. Mater. Interfaces* **2010**, *2*, 1421-1429.
- 36. Carter, M. C. D.; Wong, M. S.; Wang, F.; Lynn, D. M. Influence of Side Chain Hydrolysis on the Evolution of Nanoscale Roughness and Porosity in Amine-Reactive Polymer Multilayers. *Chem. Mater.* **2020**, *32*, 6935-6946.
- 37. Zhang, J.; Fredin, N. J.; Lynn, D. M. Erosion of Multilayered Films Fabricated from Degradable Polyamines: Characterization and Evidence in Support of a Mechanism That Involves Polymer Hydrolysis. *J. Polym. Sci., Part A: Polym. Chem.* **2006**, *44*, 5161-5173.
- 38. Cadwell, K. D.; Alf, M. E.; Abbott, N. L. Infrared Spectroscopy of Competitive Interactions between Liquid Crystals, Metal Salts, and Dimethyl Methylphosphonate at Surfaces. *J. Phys. Chem. B* **2006**, *110*, 26081-26088.
- 39. Heilmann, S. M.; Rasmussen, J. K.; Krepski, L. R. Chemistry and Technology of 2-Alkenyl Azlactones. *J. Polym. Sci., Part A: Polym. Chem.* **2001,** *39,* 3655-3677.
- 40. Cullen, S. P.; Mandel, I. C.; Gopalan, P. Surface-Anchored Poly(2-Vinyl-4,4-Dimethyl Azlactone) Brushes as Templates for Enzyme Immobilization. *Langmuir* **2008**, *24*, 13701-13709.

- 41. Buck, M. E.; Lynn, D. M. Azlactone-Functionalized Polymers as Reactive Platforms for the Design of Advanced Materials: Progress in the Last Ten Years. *Polymer Chemistry* **2012**, *3*, 66-80.
- 42. Lokitz, B. S.; Wei, J.; Hinestrosa, J. P.; Ivanov, I.; Browning, J. F.; Ankner, J. F.; Kilbey, S. M.; Messman, J. M. Manipulating Interfaces through Surface Confinement of Poly(Glycidyl Methacrylate)-Block-Poly(Vinyldimethylazlactone), a Dually Reactive Block Copolymer. *Macromolecules* **2012**, *45*, 6438-6449.
- 43. Laquièvre, A.; Allaway, N. S.; Lyskawa, J.; Woisel, P.; Lefebvre, J.-M.; Fournier, D. Highly Efficient Ring-Opening Reaction of Azlactone-Based Copolymer Platforms for the Design of Functionalized Materials. *Macromol. Rapid Commun.* **2012**, *33*, 848-855.
- 44. Li, Y.; Duong, H. T. T.; Jones, M. W.; Basuki, J. S.; Hu, J.; Boyer, C.; Davis, T. P. Selective Postmodification of Copolymer Backbones Bearing Different Activated Esters with Disparate Reactivities. *ACS Macro Lett.* **2013**, *2*, 912-917.
- 45. Jones, M. W.; Richards, S.-J.; Haddleton, D. M.; Gibson, M. I. Poly(Azlactone)s: Versatile Scaffolds for Tandem Post-Polymerisation Modification and Glycopolymer Synthesis. *Polymer Chemistry* **2013**, *4*, 717-723.
- 46. Hansen, R. R.; Hinestrosa, J. P.; Shubert, K. R.; Morrell-Falvey, J. L.; Pelletier, D. A.; Messman, J. M.; Kilbey, S. M.; Lokitz, B. S.; Retterer, S. T. Lectin-Functionalized Poly(Glycidyl Methacrylate)-Block-Poly(Vinyldimethyl Azlactone) Surface Scaffolds for High Avidity Microbial Capture. *Biomacromolecules* 2013, 14, 3742-3748.
- 47. Zhu, Y.; Batchelor, R.; Lowe, A. B.; Roth, P. J. Design of Thermoresponsive Polymers with Aqueous LCST, UCST, or Both: Modification of a Reactive Poly(2-Vinyl-4,4-Dimethylazlactone) Scaffold. *Macromolecules* **2016**, *49*, 672-680.

- 48. Rasmussen, J. K.; Heilmann, S. M.; Palensky, F. J.; Smith Ii, H. K.; Melancon, K. C. Chemistry of Alkenylazlactones, 2 Reaction with Thiols. *Die Makromolekulare Chemie, Rapid Communications* **1984**, *5*, 67-70.
- Heilmann, S. M.; Moren, D. M.; Krepski, L. R.; Pathre, S. V.; Rasmussen, J. K.; Stevens,
  J. The Chemistry of 2-Alkenyl-5(4h)-Oxazolones. VIII Acid-Catalyzed Reaction with
  Alcohols. *Tetrahedron* 1998, 54, 12151-12160.
- 50. Carter, M. C. D.; Lynn, D. M. Covalently Crosslinked and Physically Stable Polymer Coatings with Chemically Labile and Dynamic Surface Features Fabricated by Treatment of Azlactone-Containing Multilayers with Alcohol-, Thiol-, and Hydrazine-Based Nucleophiles. *Chem. Mater.* 2016, 28, 5063-5072.
- 51. Agarwal, H.; Breining, W. M.; Lynn, D. M. Continuous Fabrication of Slippery Liquid-Infused Coatings on Rolls of Flexible Materials. ACS Appl. Polym. Mater 2021; DOI: 10.1021/acsapm.1c01014.
- 52. Feng, X. J.; Jiang, L. Design and Creation of Superwetting/Antiwetting Surfaces. *Adv. Mater.* **2006**, *18*, 3063-3078.
- 53. Tian, Y.; Su, B.; Jiang, L. Interfacial Material System Exhibiting Superwettability. *Adv. Mater.* **2014**, *26*, 6872-6897.
- 54. Feng, L.; Li, S.; Li, Y.; Li, H.; Zhang, L.; Zhai, J.; Song, Y.; Liu, B.; Jiang, L.; Zhu, D. Super-Hydrophobic Surfaces: From Natural to Artificial. *Adv. Mater.* **2002**, *14*, 1857-1860.
- 55. Wong, T.-S.; Kang, S. H.; Tang, S. K. Y.; Smythe, E. J.; Hatton, B. D.; Grinthal, A.; Aizenberg, J. Bioinspired Self-Repairing Slippery Surfaces with Pressure-Stable Omniphobicity. *Nature* **2011**, *477*, 443-447.

- Solomon, B. R.; Subramanyam, S. B.; Farnham, T. A.; Khalil, K. S.; Anand, S.; Varanasi,
  K. K., Chapter 10 Lubricant-Impregnated Surfaces. In *Non-Wettable Surfaces: Theory, Preparation and Applications*, The Royal Society of Chemistry: 2017; pp 285-318.
- 57. Peppou-Chapman, S.; Hong, J. K.; Waterhouse, A.; Neto, C. Life and Death of Liquid-Infused Surfaces: A Review on the Choice, Analysis and Fate of the Infused Liquid Layer. *Chem. Soc. Rev.* **2020**, *49*, 3688-3715.
- 58. Lefort, M.; Boulmedais, F.; Jierry, L.; Gonthier, E.; Voegel, J. C.; Hemmerlé, J.; Lavalle, P.; Ponche, A.; Schaaf, P. Simultaneous Spray Coating of Interacting Species: General Rules Governing the Poly(Styrene Sulfonate)/Poly(Allylamine) System. *Langmuir* **2011**, *27*, 4653-4660.
- 59. Lefort, M.; Jierry, L.; Boulmedais, F.; Benmlih, K.; Lavalle, P.; Senger, B.; Voegel, J.-C.; Hemmerlé, J.; Ponche, A.; Schaaf, P. Nanosized Films Based on Multicharged Small Molecules and Oppositely Charged Polyelectrolytes Obtained by Simultaneous Spray Coating of Interacting Species. *Langmuir* 2013, 29, 14536-14544.

## For Table of Contents Use Only:

